Journal of Geoscience and Environment Protection, 2025, 13(10), 42-58
https://www.scirp.org/journal/gep
ISSN Online: 2327-4344
ISSN Print: 2327-4336

Diurnal and Seasonal Trends in Aerodynamic Conductance over a Grassland Surface

Ippei Iiyama

School of Agriculture, Utsunomiya University, Utsunomiya, Tochigi, Japan
Email: iiyama@cc.utsunomiya-u.ac.jp

How to cite this paper: Iiyama, I. (2025). Diurnal and Seasonal Trends in Aerodynamic Conductance over a Grassland Surface. *Journal of Geoscience and Environment Protection, 13,* 42-58.
https://doi.org/10.4236/gep.2025.1310004

Received: August 26, 2025
Accepted: October 13, 2025
Published: October 16, 2025

Abstract

The aerodynamic conductance K [m s^{-1}] is important for quantifying thermal and hydrological environments around a land surface under possible climatic scenarios. This study aimed at clarifying diurnal and seasonal trends in K [m s^{-1}] over a grassland surface. Measured data sets of air temperatures T_a [K] at two heights and wind speed u [m s^{-1}] at one height were used with the equations of the wind- and temperature-profiles. K [m s^{-1}] started increasing after sunrise, lowered steeply in late afternoon, and became stable at the daily lowest level during night, suggesting that daylength defines the time period when turbulent transport effectively occurs. The seasonal change in the diurnal pattern of K [m s^{-1}] was characterized by the transitions of the size of K [m s^{-1}] and the time of its daily peak. The daily maximum K [m s^{-1}] grew from January, became the highest of more than 0.015 [m s^{-1}] in April, and decreased through summer to winter. The time of the daily maximum K [m s^{-1}] was shifted so that it was found around 16:00 in summer and moved forward in winter. These diurnal and seasonal features of K [m s^{-1}] resembled those of friction velocity and u [m s^{-1}], suggesting that aerodynamic conductance is affected primarily by wind properties. Every month, the u-K relation drew a diurnal loop with the time of day. The loop size varied seasonally in accord with the seasonality of the sizes in u [m s^{-1}] and K [m s^{-1}], and a value of K [m s^{-1}] in the morning became two times larger or more than that in the evening for a given u [m s^{-1}]. The apparent hysteretic behavior in the diurnal u-K relation was attributable to the change in the direction of the vertical gradient in air temperature during the daytime. The non-uniqueness in the diurnal u-K relation implied that atmospheric stability needs to be considered when diurnal patterns of aerodynamic conductance are evaluated.

Keywords

Friction Velocity, Monin-Obukhov Length, Sensible Heat, Universal Similarity Function

1. Introduction

Clarifying the balances of heat and water between land and the atmosphere is important for understanding the mechanism that regulates the environments above, on, and below the land surface. Those balances can be formulated primarily through evaluating the amounts of heat and water that are exchanged between the atmosphere and the land. The amount of heat or water can be measured as a flow rate passing through a unit area during a unit time, also known as a flux. Because a value of heat- or water-flux between the two bodies is likely to be proportional to the difference in a state variable like temperature or water potential along the flow direction, the aerodynamic conductance for turbulent transfer near the land surface, as the proportionality coefficient, is an essential parameter for evaluating the fluxes of heat and water exchanged between a land surface and the atmosphere.

Of the earth's land surface, grasslands cover a large fraction, not only forming a large portion of agricultural lands, but also supplying various non-agricultural services like water supply, flow regulation, erosion control, climate mitigation, or carbon storage (Bengtsson et al., 2019), as well as nurturing global biodiversity (Murphy et al., 2016). Grasslands, savannas, and woody savannas spread out over 11×10^6 [km^2], 9×10^6 [km^2], and 10×10^6 [km^2], respectively (Loveland et al., 2000), the total of which occupies more than 20% of the earth's land surface. When the area of "grasslands" is defined by the International Vegetation Classification (IVC), more than 35×10^6 [km^2] of land areas are classified into the surface with dominant grassland types, equivalent to more than 24% of the earth's land surface (Dixon et al., 2014).

Grasslands are relatively vulnerable ecosystems to warming trends, accompanied by drought problems and various kinds of heat stress on plants, which may give negative feedback on the warming trends. For instance, rising temperatures deteriorate grass nutritive values and may cause an increase in cattle enteric methane production (Lee et al., 2017). Drought, too, lowers aboveground biomass, though improving nutritional quality as fodders (Martins-Noguerol et al., 2023).

At the same time, the effects of warming-related events may vary depending on when and how long the events are imposed on a grassland field during a growing season. For instance, warming is likely to alter phenology of grasses and forbs like lengthening reproductive duration or advancing the time of budding (Ojo et al., 2024) and, in parallel, to bring about a shift in community composition with differences in biomass and forage quality (Li et al., 2018; Martins-Noguerol et al., 2023). Drought, too, may delay budding and flowering times, leading to reduced reproductive durations (Ojo et al., 2024). The impacts of climate variability are likely to show seasonality, weakening along the progress of the growing season (Craine et al., 2012).

These studies suggest the importance of quantifying the heat- and water-balances on a grassland surface in terms of temporal behaviors. Thus, understanding temporal patterns of aerodynamic conductance is key to evaluating heat- and water-exchanges that can appear around the land surface under some climatic sce-

narios. It enables improving the usage of existing hydrological models, management of agricultural water, and forecasts for local weather.

This study aimed to evaluate diurnal and seasonal trends in aerodynamic conductance over a grassland surface. A simple procedure for evaluating aerodynamic conductance was presented, based on monitoring air temperatures at two heights and wind speed at one height, using the Monin-Obukhov similarity theory.

2. Materials and Methods

2.1. Study Sites and Measurements

Duplicate study sites "A" and "B" were set in a meadow field of 2.8 [ha] (350 × 80 [m]), called the '3-1 field' (36˚29'23"N, 139˚59'14"E), located in the Utsunomiya University Farm in Moka city, Tochigi, Japan. The study period was from May 2018 to April 2019. The grasses and forbs grown in the meadow in the study period were orchard grass (*Dactylis glomerata* L. cv. Natsumidori), tall fescue (*Festuca arundinacea* Schreb. cv. Hokuryo), hybrid ryegrass (*Lolium hybridum* Hausskn. cv. Tetrelite II), and red clover (*Trifolium pratense* L. cv. Makimidori).

The air temperatures were measured at each site at the heights of 0.7 [m] and 1.8 [m] with 30-minutes intervals by temperature loggers (HOBO U23 Pro v2 External temperature/relative humidity data logger "U23-002A"; Onset Computer Corp; Bourne, MA, USA) enveloped in radiation shields (Solar radiation shield "RS1"; Onset Computer Corp; Bourne, MA, USA). A data set of wind speed was utilized, which had been measured at 10 m in height at Moka weather station (36˚28'36"N, 139˚59'12"E; 1.4 kilometers south of the study site) (Japan Meteorological Agency, 2025).

2.2. Evaluation of Aerodynamic Conductance

The aerodynamic conductance K [m s^{-1}] was evaluated by the air temperatures T_{a1} [K] and T_{a2} [K] measured at the two heights z_{t1} = 0.7 [m] and z_{t2} = 1.8 [m], respectively, with the wind speed u_m [m s^{-1}] measured at z_u = 10 [m]. Since the combinations of T_{a1} [K], T_{a2} [K], and u_m [m s^{-1}] were obtained every 30 minutes, values of K [m s^{-1}] were evaluated with 30-minute intervals by solving a system of nonlinear equations that includes the models of the wind- and temperature-profiles in vertical direction. The wind and temperature profiles were formulated by applying the Monin-Obukhov similarity theory (Monin & Obukhov, 1954) as stated below.

2.2.1. Model of Wind Profile

According to Monin-Obukhov's theory, the vertical profile of wind speed u [m s^{-1}] above a land surface can be expressed as follows:

$$u = \frac{u_*}{k}\left(\ln\left(\frac{z-d+z_m}{z_m}\right)-\psi_m\right) \tag{1}$$

where u_* [m s^{-1}] is the friction velocity, k [−] = 0.4 is the von Karman constant, z [m] is a vertical location at which u [m s^{-1}] is given, d [m] and z_m [m] are the

height of zero plane displacement and the roughness length of momentum of the surface. And ψ_m [−] is the correction factor of atmospheric stability for momentum transfer.

Linear relations between d [m] and z_m [m] had been found on many types of air-surface interactions, while the height of plants h [m] covering the land had also been related to d [m] and z_m [m]. Maki (1975) thoroughly reviewed these relations in 16 papers and represented them with the following expressions:

$$d = a_d h \tag{2}$$

$$z_m = a_{zm} h \tag{3}$$

where the slopes a_d and a_{zm} averaged 0.717 and 0.106 among the reviewed values with their standard deviations of 0.080 and 0.045, respectively. This study adopted a_d = 0.717 and a_{zm} = 0.106, since these values allowed to approximate general trends observed for the dense canopies with all the variety of conditions (Maki, 1975). The time series of h [m] was approximated as a sequence of linear functions of time based on such observations that the first, second, and third cuttings of the crops in the study field were done on 5/24, 7/25, and 9/24 in 2018, and the height of plants returned to about 0.1 [m] on each cutting date, while it reached around 0.5 [m] during each growing period. On these settings, d [m] and z_m [m] were regarded as known variables that were specified for a given plant height h [m].

The ψ_m [−] in Equation (1) is defined by using the universal similarity function for momentum transfer φ_m [−] as follows:

$$\psi_m(x) = \psi_m(x_0) + \int_{x_0}^{x} \frac{1-\varphi_m(x)}{x} \mathrm{d}x \tag{4}$$

where x [−] is an auxiliary variable defined as the ratio of $z-d$ [m] to the Monin-Obukhov length L [m] (Monin & Obukhov, 1954), and the integrand φ_m [−] was of one of the existing models as below (Paulson, 1970; Dyer, 1974):

$$\varphi_m(x) = \begin{cases} 1+5x & (L \geq 0) \\ (1-16x)^{-0.25} & (L < 0) \end{cases} \tag{5}$$

And, by assuming that x_0 [−] in Equation (4) is negligibly small, ψ_m [−] is formulated as below:

$$\psi_m(x) \approx \begin{cases} -5x & (L \geq 0) \\ \ln f_m(y) - 2\tan^{-1} y + \dfrac{\pi}{2} & (L < 0) \end{cases} \tag{6}$$

where $y = (1-16x)^{0.25}$ and $f_m(y) = \left((1+y)/2\right)^2 \left(1+y^2\right)/2$.

Equations (4) through (6) show that a value of ψ_m [−] is identified when values of d [m], L [m], and z [m] are given. As mentioned above, d [m] and z_m [m] in this study were known variables. Thus, when a pair of $u = u_m$ [m s^{-1}] and $z = z_u$ [m] are given as measured values, unknown variables in Equation (1) are u_* [m s^{-1}] and L [m]. And, as explained below, L [m] can be expressed as a function of the sensible heat flux from the surface to the atmosphere H [W m^{-2}], the friction velocity u_* [m s^{-1}], the air temperature T_a [K], and the atmospheric pressure p_a

[Pa]. This means that H [W m^{-2}] and u_* [m s^{-1}] are unknown variables for L [m] under a given weather condition and, in turn, that the unknown variables in Equation (1) are H [W m^{-2}] and u_* [m s^{-1}] under the given weather condition.

The Monin-Obukhov length L [m] is formulated as below (Monin & Obukhov, 1954):

$$L = -\left(\frac{\tau}{\rho_a}\right)^{\frac{3}{2}} \frac{C_h T_{ave}}{kgH} \tag{7}$$

where τ [N s m^{-2} s^{-1}] is the momentum flux, ρ_a [kg m^{-3}] is the density of air, g [m s^{-2}] is the acceleration of the earth's gravity, H [W m^{-2}] is the sensible heat flux from the surface to the atmosphere, T_{ave} [K] is the average temperature in the air layer of interest, and C_h [J m^{-3} K^{-1}] is the volumetric heat capacity of air. Equation (7) was derived with the assumption that spatial variation in temperature in the air layer is small compared with T_{ave} [K]. Because the u_* [m s^{-1}] in Equation (1) is defined as the square root of the ratio of τ [N s m^{-2} s^{-1}] to ρ_a [kg m^{-3}] (Monin & Obukhov, 1954), Equation (7) can be rearranged as below:

$$L = -u_*^3 \frac{C_h T_{ave}}{kgH} \tag{8}$$

The C_h [J m^{-3} K^{-1}] in Equation (8) is defined as the density of air ρ_a [kg m^{-3}] multiplied by the specific heat of air c_p [J kg^{-1} K^{-1}]:

$$C_h = \rho_a c_p \tag{9}$$

The ρ_a [kg m^{-3}] was approximately quantified by using the ideal gas law as follows:

$$\rho_a = \frac{p_a M_a}{R T_a} \tag{10}$$

where T_a [K] and p_a [Pa] are air temperature and atmospheric pressure, M_a [kg mol^{-1}] is the molar weight of the air ($\fallingdotseq$ 0.028 966 [kg mol^{-1}]), R [J mol^{-1} K^{-1}] is the ideal gas constant (= 8.314 [J mol^{-1} K^{-1}]). The c_p [J kg^{-1} K^{-1}], too, was described as a function of T_a [K] and p_a [Pa] by applying the multivariate regression to the data set tabulated in Lemmon (2010):

$$c_p = a_0 + a_1 T_a + a_2 p_a \tag{11}$$

where a_0, a_1, and a_2 are 1120.42 [J kg^{-1} K^{-1}], −0.369 05 [J kg^{-1} K^{-2}], and 15.5494 × 10^{-6} [J kg^{-1} K^{-1} Pa^{-1}], respectively. The coefficient of determination R^2 of Equation (11) was 0.909 53. As shown in Equations (8) through (11), the L [m] is a function of H [W m^{-2}], u_* [m s^{-1}], T_a [K], and p_a [Pa], meaning that H [W m^{-2}] and u_* [m s^{-1}] are unknown variables for L [m] under a given weather condition.

In summation, Equation (1) should hold true when a proper pair of H [W m^{-2}] and u_* [m s^{-1}] is found when a set of relevant measured values is given.

2.2.2. Model of Temperature Profile

As Equation (1) is formulated, the vertical profile of temperature T_a [K] is ex-

pressed as follows:

$$T_a = T_s - \frac{H}{kC_h u_*}\left(\ln\frac{z-d+z_h}{z_h} - \psi_h\right) \tag{12}$$

where T_s [K] is the temperature at $z = d$ [m], the z_h [m] is the roughness length of heat on the land surface. Some linear relations between z_h [m] and z_m [m] had been proposed (Garratt & Francey, 1978; Shaw & Pereira, 1982), and the ratio of z_h [m] to z_m [m] is likely to take a value between 0.1 and 0.2. Among the linear relations, Garratt & Francy (1978) found such a relation as:

$$\ln\frac{z_m}{z_h} \approx 2 \tag{13}$$

by plotting $\ln(z_m/z_h)$ against the roughness Reynolds number Re_* (= $u_* z_m/\nu$, where ν [$\mathrm{m^2\ s^{-1}}$] is the kinematic viscosity of air) in the range $10 < \mathrm{Re}_* < 10^5$ for various types of surfaces, including bare soil, grass and crops, shrubs, and forested area.

The ψ_h [−], the stability correction factor for heat transfer, was also introduced. The derivation process of ψ_h [−] is like that of ψ_m [−] as follows:

$$\psi_h(x) = \psi_h(x_0) + \int_{x_0}^{x}\frac{1-\varphi_h(x)}{x}\mathrm{d}x \tag{14}$$

The definition of the auxiliary parameter x [−] in Equation (14) is the same as that in Equation (4). The universal similarity function for heat transfer φ_h [−] is expressed in the same manner as φ_m [−] as follows (Dyer, 1974):

$$\varphi_h(x) = \begin{cases} 1+5x & (L \geq 0) \\ (1-16x)^{-0.5} & (L < 0) \end{cases} \tag{15}$$

And, for a very small x_0 [−] in Equation (14), the resultant ψ_h [−] can be calculated as below:

$$\psi_h(x) \approx \begin{cases} -5x & (L \geq 0) \\ \ln f_h(y) & (L < 0) \end{cases} \tag{16}$$

where $f_h(y) = \left(\left(1+y^2\right)/2\right)^2$, and $y = (1-16x)^{0.25}$ as defined in Equation (6).

When the variables in Equation (12) are classified into variables with given values and unknown variables in the same way as those in Equation (1), it is noticed that Equation (12) should hold true when a proper set of H [$\mathrm{W\ m^{-2}}$], T_s [K] and u_* [$\mathrm{m\ s^{-1}}$] is identified for a series of measured values.

2.2.3. System of Equations for Evaluating Aerodynamic Conductance

As formulated above, Equations (1) and (12) can coincidentally hold true when an adequate set of H [$\mathrm{W\ m^{-2}}$], T_s [K], and u_* [$\mathrm{m\ s^{-1}}$] are input for a given set of relevant measured values. This means that three equations are required for identifying the unknowns H [$\mathrm{W\ m^{-2}}$], T_s [K], and u_* [$\mathrm{m\ s^{-1}}$]. Therefore, this study used the following three equations:

$$\begin{cases} u_m = \dfrac{u_*}{k}\left(\ln\left(\dfrac{z_u - d + z_m}{z_m}\right) - \psi_m\right) \\ T_{a1} = T_s - \dfrac{H}{kC_h u_*}\left(\ln\dfrac{z_{t1} - d + z_h}{z_h} - \psi_{h1}\right) \\ T_{a2} = T_s - \dfrac{H}{kC_h u_*}\left(\ln\dfrac{z_{t2} - d + z_h}{z_h} - \psi_{h2}\right) \end{cases} \tag{17}$$

Because Equation (17) is a system of nonlinear equations, the Newton-Raphson iterative scheme was adopted to solve it.

Finally, every time a set of H [W m^{-2}] and T_s [K] was determined, the aerodynamic conductance K [m s^{-1}] was obtained by using the following expression:

$$K = \frac{H}{C_h\left(T_s - T_a\right)} \tag{18}$$

3. Results and Discussion

3.1. Temporal Patterns of the Measured Weather Conditions

Figure 1 shows the time series of air temperatures observed every 30 minutes in the two sites. T_{a1} [K] and T_{a2} [K] denote the air temperatures monitored at 0.7 [m] and 1.8 [m] in height at each site, respectively. The sensor at 0.7 [m] in height in site A had failed to record the data due to a battery trouble from 2018/8/19 19:00 to 2018/10/15 12:00 and from 2019/4/24 5:00 to 2019/4/30 23:30. The portion of the data obtained at 0.7 [m] in height in site B had also been lost from 2018/10/28 4:30 to 2018/12/28 13:00.

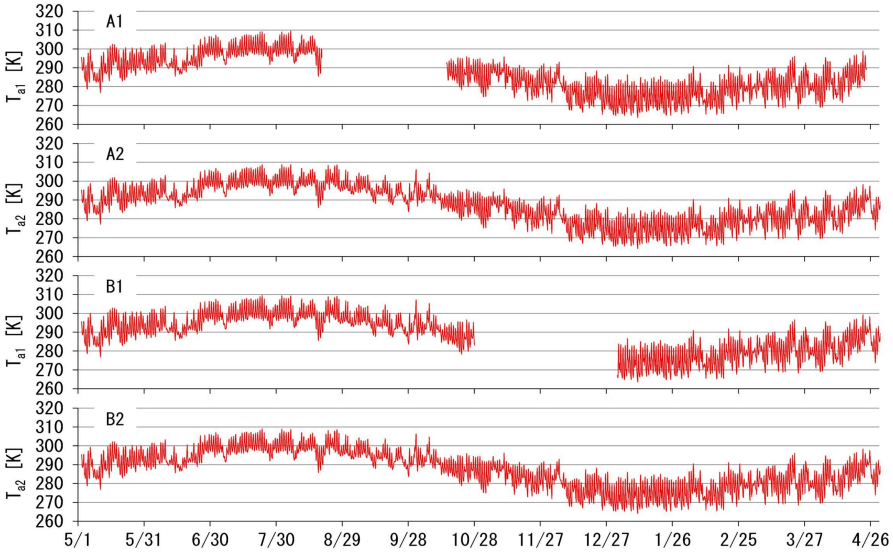

Figure 1. The time series of the measured air temperatures. The sub-graphs A1 and A2 show the temperatures obtained at the heights of 0.7 [m] (T_{a1} [K]) and 1.8 [m] (T_{a2} [K]) in site A, respectively. The sub-graphs B1 and B2 show the values obtained at the two heights in site B.

The curves together showed annual peaks around 300 [K] in July and found bottoms around 275 [K] in January. And the daily ranges were roughly 10 to 20 degrees, being larger in winter than in summer. These four temperature records showed almost the same patterns, and the features of the four data sets had no clear distinctions among them. In fact, the diurnal trends of the four data sets were almost the same as each other (Figure 2), in which the daily maxima and minima appeared around 15:00 and the sunrise, respectively, regardless of season, and the daily ranges narrowed in summer and widened in winter.

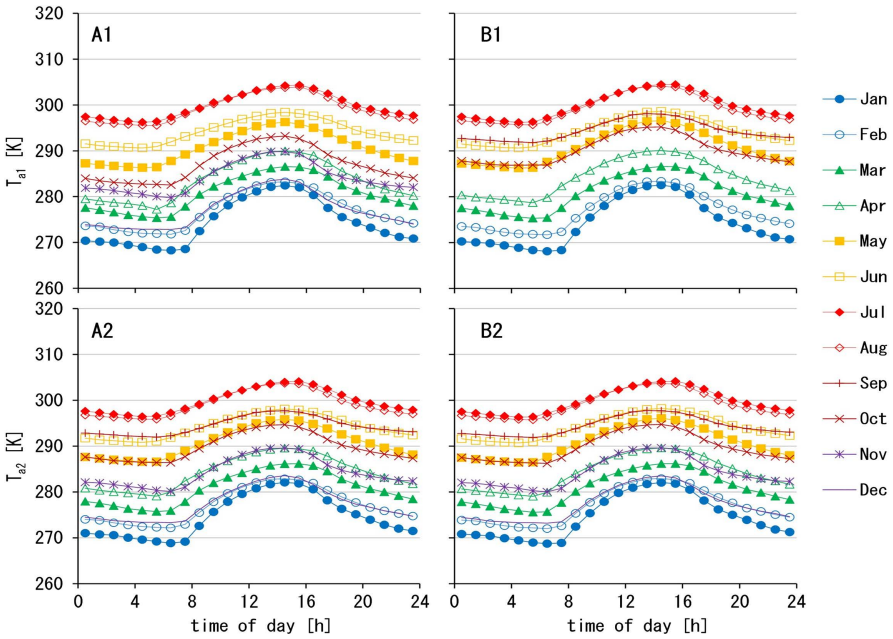

Figure 2. The diurnal changes in the air temperatures T_{a1} [K] and T_{a2} [K]. The sub-graphs' names are given in the same manner as in Figure 1. The plots were derived in such a way that (i) each of the four data sets on Figure 1 is separated into 12 parts with one-month interval, (ii) each monthly data set is sorted in time-of-day order with one-hour interval, (iii) the values found in each one-hour interval were averaged, and (iv) monthly-averaged hourly values were plotted for each of 12 months. The months of the data loss were omitted from the analyses so that no bias can be introduced into any of the monthly-averaged values.

However, the temperature difference $T_{a2} - T_{a1}$ [K] clearly showed that the two temperatures had literally differed from each other (Figure 3(i)), fluctuating between −1 and +2 degrees. It took smaller values in warmer seasons, while large upward temperature gradients were found mainly in winter. And, their monthly-averaged diurnal patterns (Figure 3(ii)) showed that $T_{a2} - T_{a1}$ [K] became positive mainly at night, causing the air on the land surface to be stable, suggesting that the size of the aerodynamic conductance reduced during the nights. On the other hand, the negative values were observed during the daytime for every month, with a peak one hour before the daily maximum temperature. These implied that upward sensible heat flux appeared solely during daytime, while almost no sensible heat flux was found during nighttime due to a very stable atmospheric condition.

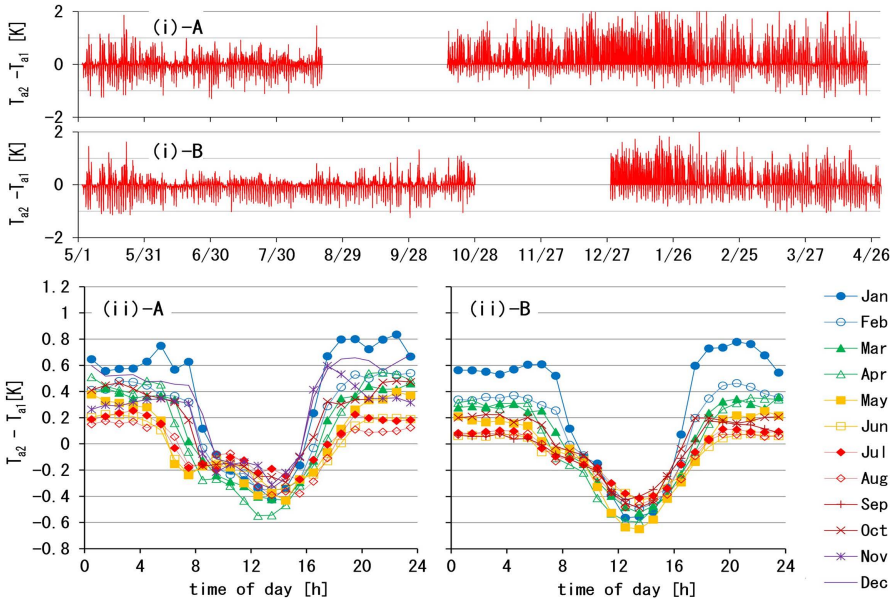

Figure 3. The time series of the temperature difference $T_{a2} - T_{a1}$ [K] for the sites A ((i)-A) and B ((i)-B), derived from the data sets depicted on **Figure 1**, with the monthly-averaged diurnal patterns of the $T_{a2} - T_{a1}$ [K] for the sites A ((ii)-A) and B ((ii)-B). The sub-graphs (ii)-A and (ii)-B were obtained by rearranging and plotting the data sets in the sub-graphs (i)-A and (i)-B in the same manner as shown in the explanatory note for **Figure 2**.

The wind speed fluctuated primarily between 0 and 5 [m s^{-1}] regardless of season, and occasionally took more than 5 [m s^{-1}] during the study period (**Figure 4(i)**). However, it became strong from spring to early summer and weakened from late autumn to winter, according to its monthly-averaged diurnal patterns (**Figure 4(ii)**). In addition, unlike the trends found on the air temperature measurements, the peak time of the wind speed had moved forward from around 16:00 in spring to around 13:00 in winter.

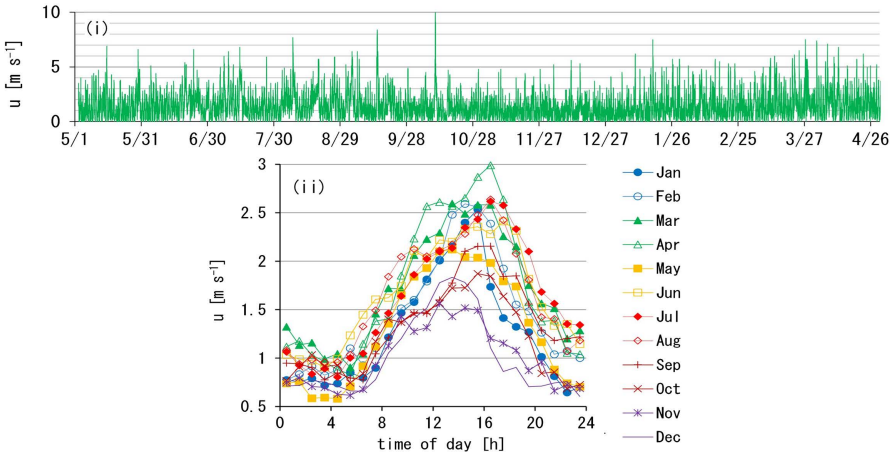

Figure 4. (i) The time series and (ii) the diurnal patterns of the wind speed u [m s^{-1}]. The latter is drawn by rearranging the former in the same way as explained in **Figure 2**. The temporal average and the standard deviation of the data set on the sub-graph (i) are 1.42 [m s^{-1}] and 1.14 [m s^{-1}], respectively.

3.2. Time Series and Diurnal Patterns of the Evaluated Quantities

Figure 5 shows the time series of the sensible heat flux H [W m^{-2}] upward positive, the temperature at the height of zero plane displacement T_s [K], the friction velocity u_* [m s^{-1}], and the aerodynamic conductance K [m s^{-1}], which were evaluated by solving Equations (17) and (18) for the measured data sets on Figure 1 and Figure 4(i).

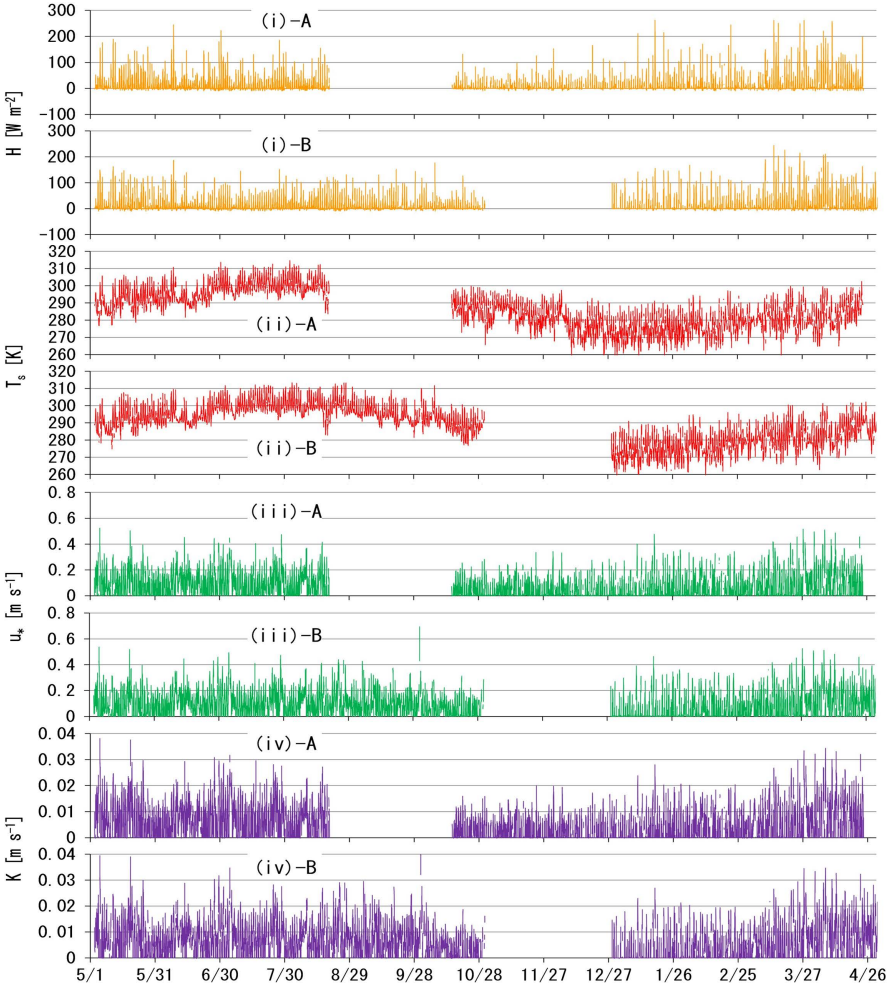

Figure 5. The time series of (i) the sensible heat flux H [W m^{-2}], (ii) the temperature at the height of zero plane displacement T_s [K], (iii) the friction velocity u_* [m s^{-1}], and (iv) the aerodynamic conductance K [m s^{-1}]. Each of the sub-indices "A" and "B" denotes the study site name for the plotted data sets.

The values of H [W m^{-2}] (Figure 5(i)) ranged from −9.8 to 262.6 [W m^{-2}] for the site A, while those for the site B fell between −9.7 and 243.7 [W m^{-2}]. The temporal averages of H [W m^{-2}] were 9.1 and 11.8 [W m^{-2}] with the standard deviations of 24.5 and 26.2 [W m^{-2}] in sites A and B, respectively. The median of H [W m^{-2}] for each site was 0.0 [W m^{-2}], meaning that the number of the data points with positive H [W m^{-2}] was almost equivalent to that with negative H [W m^{-2}] and, thus, large positive values in H [W m^{-2}] occurred very occasionally, though many data

points with $H > 50$ [W m^{-2}] were found.

The time series of T_s [K] (**Figure 5(ii)**) showed almost the same patterns of annual cycle as the measured air temperatures T_{a1} [K] and T_{a2} [K] in **Figure 1**. However, the daily ranges of T_s [K] were larger than those of T_{a1} [K] and T_{a2} [K] throughout the study period, certainly driving the sensible heat flux H [W m^{-2}] in either upward or downward direction by making the temperature difference in Equation (17) significant.

The friction velocity u_* [m s^{-1}] (**Figure 5(iii)**) fluctuated between 0.00 and 0.52 [m s^{-1}] in site A and 0.00 and 0.69 [m s^{-1}] in site B in the study period. The temporal averages of u_* [m s^{-1}] were 0.08 and 0.09 [m s^{-1}] with the standard deviations of 0.09 and 0.09 [m s^{-1}] in sites A and B, respectively. The medians of 0.04 and 0.07 [m s^{-1}] for sites A and B indicated that the small number of large values pulled up the averages.

The aerodynamic conductance K [m s^{-1}] (**Figure 5(iv)**) fluctuated mainly between 0.00 and 0.02 [m s^{-1}] and rarely exceeded 0.03 [m s^{-1}] during the study period, with the annual averages of 0.0051 and 0.0064 [m s^{-1}] in sites A and B, respectively. These values were one-digit smaller than those found on forests of juniper (Duman et al., 2021) or of spruce (Hurtalova et al., 2005), and about half of those found on tall aquatic plants (Hemes et al., 2018), suggesting the positive relation between h [m] and K [m s^{-1}].

The diurnal patterns of H [W m^{-2}], T_s [K], u_* [m s^{-1}], and K [m s^{-1}] were displayed in **Figure 6**. All the parameters rose after sunrise and fell toward sunset every month, and the diurnal cycle changed gradually in height and length from month to month. As a result, the diurnal patterns of the four parameters showed some seasonal cycles.

Particularly, the aerodynamic conductance K [m s^{-1}] (**Figure 6(iv)**) rose only in daytime and stayed below a daily average with almost a constant value during night. Every month, the value of K [m s^{-1}] sharply increased just after sunrise, and then, the rate of increase in K [m s^{-1}] became moderate until K [m s^{-1}] reached its daily peak. After that, K [m s^{-1}] lowered steeply by the time it got dark. Thus, it can be said that the times of sunrise and sunset define the seasonal contraction and expansion of the period when K [m s^{-1}] effectively promotes the heat exchange between the land and the atmosphere.

The daytime K [m s^{-1}] showed such a seasonality that it grew in spring, slightly declined in summer, and steeply reduced through autumn to winter, while the nighttime K [m s^{-1}] was larger in warmer seasons and got close to zero in winter. In this annual cycle, the daily maximum of K [m s^{-1}] peaked in April, reaching beyond 0.015 [m s^{-1}], and started dropping in the warmest season, reduced through autumn, and bottomed out amid winter. The time of the daily maximum K [m s^{-1}] also shifted from season to season, which was found around 16:00 in summer and moved forward in winter.

3.3. Relations among the Aerodynamic Conductance and Wind

The diurnal and seasonal features of K [m s^{-1}] resembled those of u_* [m s^{-1}] as

closely as the shapes of the curves on Figure 6(iii) were like those on Figure 6(iv), while they were different from the diurnal and seasonal patterns of T_a [K] (Figure 2) and T_s [K] (Figure 6(ii)). These evaluations suggested that u_* [m s^{-1}] or the wind speed u [m s^{-1}] is the principal environmental variable for defining K [m s^{-1}], though the air temperatures surely affect the size of K [m s^{-1}] as the theory behind Equations (17) and (18) tells.

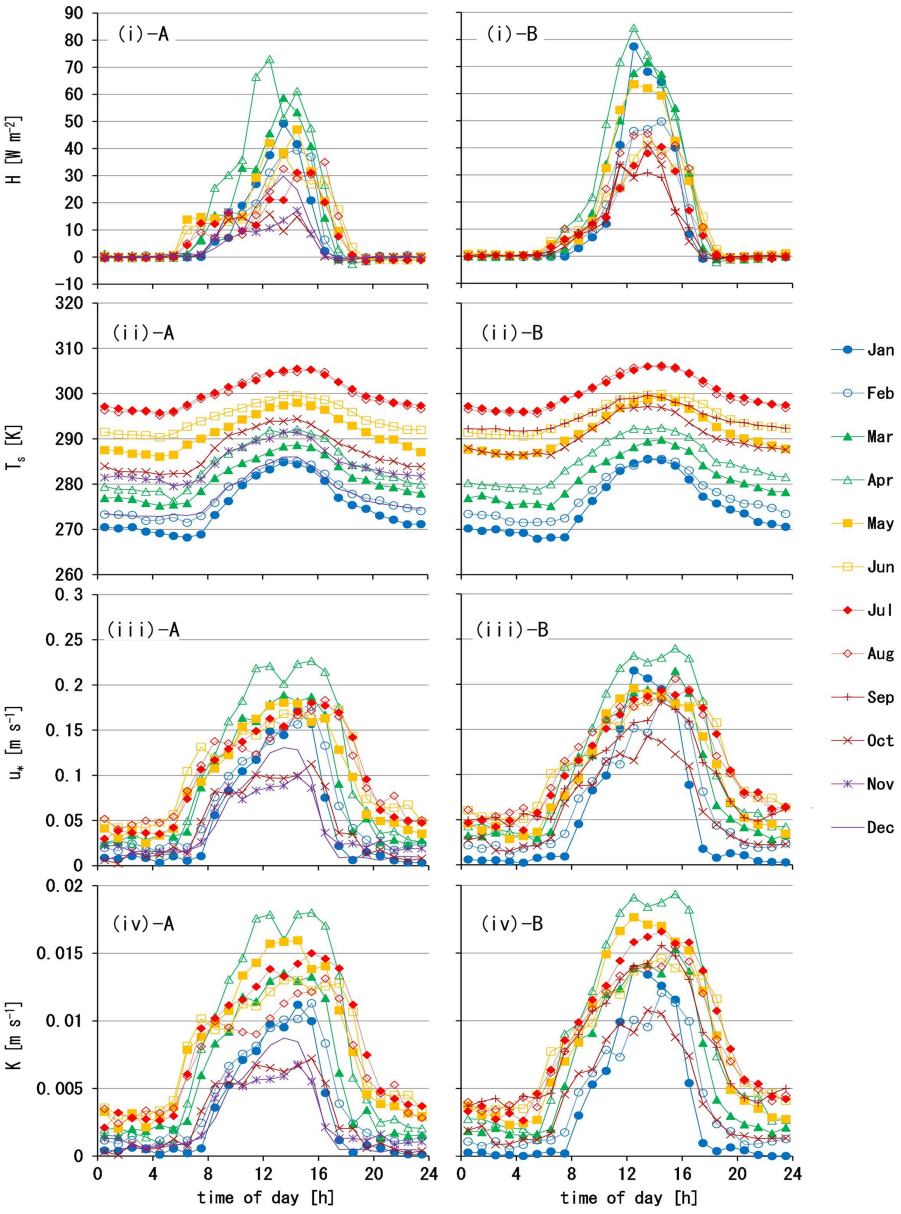

Figure 6. The diurnal patterns of (i) the sensible heat flux H [W m^{-2}], (ii) the temperature at the height of zero plane displacement T_s [K], (iii) the friction velocity u_* [m s^{-1}], and (iv) the aerodynamic conductance K [m s^{-1}]. The sub-indices "A" and "B" denote the names of the study sites. Each sub-graph is drawn by rearranging the corresponding data set in Figure 5 in the same manner as explained in Figure 2.

In fact, the comparisons of the values of u_* [m s^{-1}] on Figure 6(iii) with those

of K [m s^{-1}] on Figure 6(iv) gave a linear relationship expressed as below:

$$K = bu_* \tag{19}$$

The value of the proportionality coefficient b [−] obtained by fitting Equation (19) to the whole-year data set of u_*-K relation was 0.075 for the site A, while that for the site B was 0.077, with the coefficient of determination $R^2 = 0.989$ for any of the two sites. When b [−] was determined for an every-month data set, it varied with such an annual cycle that it took its minimum of 0.065 in January and its maximum of 0.088 in May, with R^2 being consistently more than 0.999. These features implied that once a pair of u_* [m s^{-1}] and K [m s^{-1}] is obtained, a value of K [m s^{-1}] at any other time can be estimated solely by evaluating u_* [m s^{-1}] through wind profile measurements, and monitoring air temperatures can no longer be required. Of course, a pair of u_* [m s^{-1}] and K [m s^{-1}] obtained once a month can give more precise estimations of K [m s^{-1}] in each month.

Since K [m s^{-1}] and u_* [m s^{-1}] seemed to be cognate parameters derived from the wind speed u [m s^{-1}], the relation between K [m s^{-1}] and u [m s^{-1}] was also probed (Figure 7). Every curve of the u-K relation was made for every one-month data set by matching the values of K [m s^{-1}] on Figure 6(iv) against the values of u [m s^{-1}] on Figure 4(ii) in order of the time of day. Any of the u-K relations formed a diurnal loop with a clockwise trajectory with time on the graph. And the loop size varied seasonally, reflecting the seasonality of the sizes in u [m s^{-1}] and K [m s^{-1}]. In many of the loops, a value of K [m s^{-1}] in the morning often became two times larger or more than that in the evening for a given u [m s^{-1}].

The theory that gives the wind- and temperature-profiles of Equations (1) and (12) indicates that K [m s^{-1}] can be expressed as a multiple of u [m s^{-1}] mediated by u_* [m s^{-1}]. However, as Equations (6) and (16) express, the relation between u [m s^{-1}] and K [m s^{-1}] is not unique and, instead, is defined by two different sets of expressions depending on whether the atmosphere is stable or not and on the extent of the atmospheric stability measured by the Monin-Obukhov length L [m]. For instance, the times of day at which u [m s^{-1}] took 1.5 [m s^{-1}] in July were around 8:00 and around 21:00 (Figure 4(ii)), while the vertical gradient of air temperature in July was negative at 8:00 and reversed its direction before 21:00 (Figure 3(ii)), resulting in two different values in K [m s^{-1}] for the single u [m s^{-1}]. In addition, it can be found on Figure 3(ii) and Figure 4(ii) that the time of daily maximum u [m s^{-1}] did not coincide with the time of daily maximum $T_{a2} - T_{a1}$ [K], meaning that the diurnal pattern in $T_{a2} - T_{a1}$ [K] slightly differed in temporal phase from that in u [m s^{-1}] in any month. This feature can also explain the cause of the loop-like behaviors in the u-K relations. Consequently, it can be said that the loop-like behavior of the u-K relation owes to the temporal phase lag between the diurnal peak of u [m s^{-1}] and the vertical temperature gradient $\mathrm{d}T_a/\mathrm{d}z$ [K m^{-1}]. The loop-like behavior of the u-K relation may be called a hysteretic behavior, because the u-K relations differed between the processes with $\mathrm{d}K/\mathrm{d}u > 0$ and with $\mathrm{d}K/\mathrm{d}u < 0$. However, since there was such a true cause for the two different u-K paths as the change in the sign of $\mathrm{d}T_a/\mathrm{d}z$, the expression "a hysteretic behavior" can be quali-

fied with the adjective "apparent". In any case, it holds true that to know the diurnal patterns of aerodynamic conductance requires the consideration of the effects of the atmospheric stability, instead of simply assuming the atmospheric condition is neutral.

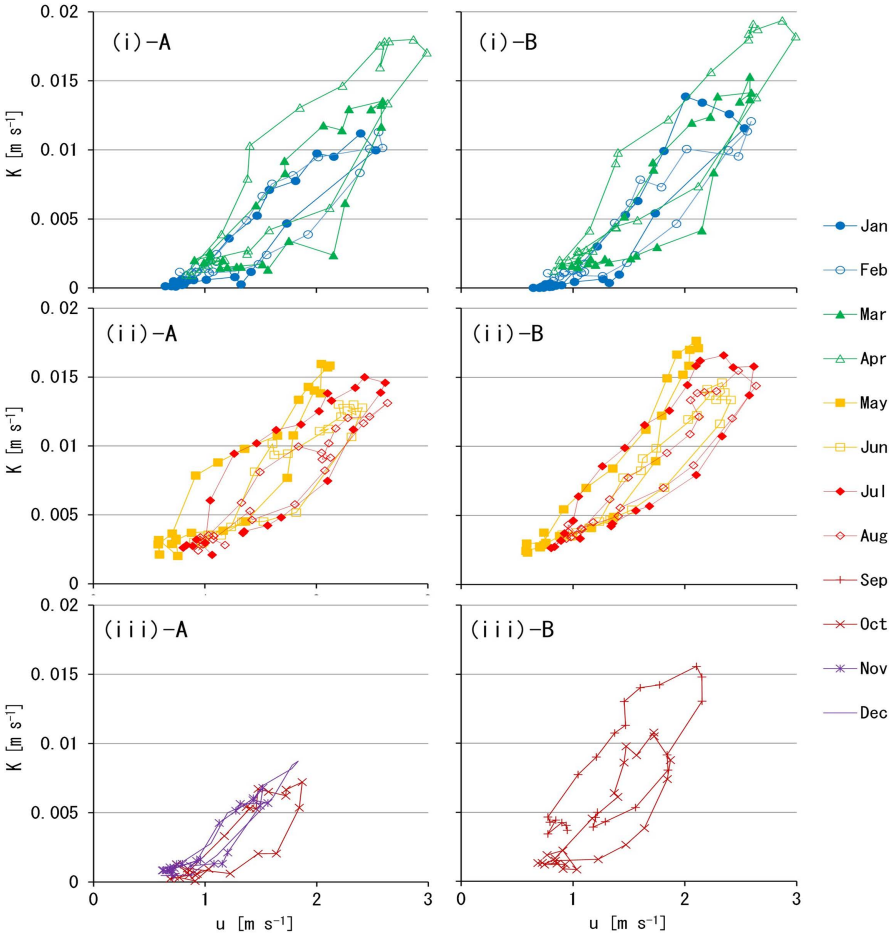

Figure 7. The relations between the wind speed u [m s^{-1}] and the aerodynamic conductance K [m s^{-1}]. Each curve is made for a one-month data set by combining the values of u [m s^{-1}] on **Figure 4(ii)** with those of K [m s^{-1}] on **Figure 6(iv)**, so that a plot is made for a time of day and connected to other plots in order of the time of day. To avoid the intricacy of too many plots overlaying each other in a single graph, all the data are divided into three classes so that the sub-graphs (i), (ii), and (iii) correspond to the first, second, and third four-month periods, respectively. "A" and "B" in the sub-graphs' names denote the study site names.

4. Conclusion

The temporal pattern of the aerodynamic conductance K [m s^{-1}] is a basic feature for quantifying the heat- and water-balances on a grassland surface and, thus, is important for both knowing current heat- and water-exchanges and predicting thermal and hydrological environments around the land surface under possible climatic scenarios. Therefore, this study evaluated diurnal and seasonal trends of K [m s^{-1}] over a grassland surface by using the measured data sets of air tempera-

tures T_a [K] at two heights and wind speed u [m s^{-1}] at one height. For the evaluation, the equations of the wind- and temperature-profiles were derived from the Monin-Obukhov similarity theory, the solutions of which were the sensible heat flux H [W m^{-2}], the temperature at the height of zero plane displacement T_s [K], and the friction velocity u_* [m s^{-1}].

The aerodynamic conductance K [m s^{-1}] took significant values mainly in daytime, while its nighttime values were consistently less than 0.005 [m s^{-1}] every month, showing such a clear diurnal pattern that K [m s^{-1}] sharply increases just after sunrise, lowers steeply by sunset, and becomes stable at the daily lowest level during night. As a result, the time period when K [m s^{-1}] effectively promotes the turbulent transport on the surface should contract and expand in accordance with the seasonal change in the times of sunrise and sunset.

The diurnal pattern of K [m s^{-1}] varied seasonally in terms of the size of K [m s^{-1}] and the time of its daily peak. The maximum size in daytime K [m s^{-1}] grew from January, became the highest of more than 0.015 [m s^{-1}] in April, and decreased through summer to winter. The time of the daily peak in K [m s^{-1}] was shifted so that it was found around 16:00 in summer and moved forward in winter.

These diurnal and seasonal features of K [m s^{-1}] resembled those of u_* [m s^{-1}] and u [m s^{-1}], suggesting that u_* [m s^{-1}] or u [m s^{-1}] is the principal environmental variable for defining K [m s^{-1}], though the air temperatures certainly influence the size of K [m s^{-1}] as expressed in the theory including the Monin-Obukhov length L [m]. In fact, the u_*-K relation was expressed clearly by a linear function $K = bu_*$, implying that once a pair of u_* [m s^{-1}] and K [m s^{-1}] is obtained, a value of K [m s^{-1}] at any other time can be estimated solely by evaluating u_* [m s^{-1}] through wind profile measurements.

At the same time, every u-K relation drew a diurnal loop with the time of day. The loop size varied seasonally in accord with the seasonality of the sizes in u [m s^{-1}] and K [m s^{-1}], while a value of K [m s^{-1}] in the morning became two times larger or more than that in the evening for a given u [m s^{-1}]. Therefore, it holds true that knowing the diurnal patterns of aerodynamic conductance requires considering the effects of atmospheric stability instead of simply assuming the atmospheric condition is neutral. In addition, this loop-like behavior of the u-K relation was attributable to the change in the direction of the vertical gradient in air temperature $\mathrm{d}T_a/\mathrm{d}z$, during the daytime. Therefore, although the loop-like behavior found on the u-K relation may be called a hysteretic behavior as the two different pathways were recognized between the processes of $\mathrm{d}K/\mathrm{d}u > 0$ and of $\mathrm{d}K/\mathrm{d}u < 0$, it can be called an "apparent" hysteresis of the u-K relation.

Conflicts of Interest

The author declares no conflicts of interest regarding the publication of this paper.

References

Bengtsson, J., Bullock, J. M., Egoh, B., Everson, C., Everson, T., O'Connor, T. et al. (2019).

Grasslands—More Important for Ecosystem Services than You Might Think. *Ecosphere, 10,* e02582. https://doi.org/10.1002/ecs2.2582

Craine, J. M., Nippert, J. B., Elmore, A. J., Skibbe, A. M., Hutchinson, S. L., & Brunsell, N. A. (2012). Timing of Climate Variability and Grassland Productivity. *Proceedings of the National Academy of Sciences, 109,* 3401-3405. https://doi.org/10.1073/pnas.1118438109

Dixon, A. P., Faber-Langendoen, D., Josse, C., Morrison, J., & Loucks, C. J. (2014). Distribution Mapping of World Grassland Types. *Journal of Biogeography, 41,* 2003-2019. https://doi.org/10.1111/jbi.12381

Duman, T., Huang, C., & Litvak, M. E. (2021). Recent Land Cover Changes in the Southwestern US Lead to an Increase in Surface Temperature. *Agricultural and Forest Meteorology, 297,* Article 108246. https://doi.org/10.1016/j.agrformet.2020.108246

Dyer, A. J. (1974). A Review of Flux-Profile Relationships. *Boundary-Layer Meteorology, 7,* 363-372. https://doi.org/10.1007/bf00240838

Garratt, J. R., & Francey, R. J. (1978). Bulk Characteristics of Heat Transfer in the Unstable, Baroclinic Atmospheric Boundary Layer. *Boundary-Layer Meteorology, 15,* 399-421. https://doi.org/10.1007/bf00120603

Hemes, K. S., Eichelmann, E., Chamberlain, S. D., Knox, S. H., Oikawa, P. Y., Sturtevant, C. et al. (2018). A Unique Combination of Aerodynamic and Surface Properties Contribute to Surface Cooling in Restored Wetlands of the Sacramento-San Joaquin Delta, California. *Journal of Geophysical Research: Biogeosciences, 123,* 2072-2090. https://doi.org/10.1029/2018jg004494

Hurtalova, T., Matejka, F., Janous, D., Roznovsky, J., & Markova, I., (2005). Wind Speed and Aerodynamic Conductance Variation in Air Layer Affected by Spruce Forest Stand. *Contributions to Geophysics and Geodesy, 35,* 319-330.

Japan Meteorological Agency (2025). *Weather Station Data Search.* http://www.jma.go.jp/jma/en/quickinfo/quickinfo.html

Lee, M. A., Davis, A. P., Chagunda, M. G. G., & Manning, P. (2017). Forage Quality Declines with Rising Temperatures, with Implications for Livestock Production and Methane Emissions. *Biogeosciences, 14,* 1403-1417. https://doi.org/10.5194/bg-14-1403-2017

Lemmon, E. W. (2010). Thermophysical Properties of Air. In W. M. Haynes, & D. R. Lide (Eds.), *CRC Handbook of Chemistry and Physics* (91st ed., pp. 615-637). CRC Press.

Li, C., Peng, F., Xue, X., You, Q., Lai, C., Zhang, W. et al. (2018). Productivity and Quality of Alpine Grassland Vary with Soil Water Availability under Experimental Warming. *Frontiers in Plant Science, 9,* Article ID: 1790. https://doi.org/10.3389/fpls.2018.01790

Loveland, T. R., Reed, B. C., Brown, J. F., Ohlen, D. O., Zhu, Z., Yang, L. et al. (2000). Development of a Global Land Cover Characteristics Database and IGBP Discover from 1 Km AVHRR Data. *International Journal of Remote Sensing, 21,* 1303-1330. https://doi.org/10.1080/014311600210191

Maki, T. (1975). Interrelationships between Zero-Plane Displacement, Aerodynamic Roughness Length and Plant Canopy Height. *Journal of Agricultural Meteorology, 31,* 7-15. https://doi.org/10.2480/agrmet.31.7

Martins-Noguerol, R., Moreno-Pérez, A. J., Pedroche, J., Gallego-Tévar, B., Cambrollé, J., Matías, L. et al. (2023). Climate Change Alters Pasture Productivity and Quality: Impact on Fatty Acids and Amino Acids in Mediterranean Silvopastoral Ecosystems. *Agriculture, Ecosystems & Environment, 358,* Article 108703. https://doi.org/10.1016/j.agee.2023.108703

Monin, A. S., & Obukhov, A. M. (1954). Basic Laws of Turbulent Mixing in the Surface

Layer of the Atmosphere. *Труды Академии Наук СССР Геофизического Института, 24,* 163-187.

Murphy, B. P., Andersen, A. N., & Parr, C. L. (2016). The Underestimated Biodiversity of Tropical Grassy Biomes. *Philosophical Transactions of the Royal Society B: Biological Sciences, 371,* Article 20150319. https://doi.org/10.1098/rstb.2015.0319

Ojo, T. A., Kirkman, K., & Tedder, M. (2024). Effects of Warming and Rainfall Variation on Grass Phenology and Regenerative Responses in Mesic Grassland. *South African Journal of Botany, 174,* 107-115. https://doi.org/10.1016/j.sajb.2024.08.050

Paulson, C. A. (1970). The Mathematical Representation of Wind Speed and Temperature Profiles in the Unstable Atmospheric Surface Layer. *Journal of Applied Meteorology, 9,* 857-861. https://doi.org/10.1175/1520-0450(1970)009<0857:tmrows>2.0.co;2

Shaw, R. H., & Pereira, A. R. (1982). Aerodynamic Roughness of a Plant Canopy: A Numerical Experiment. *Agricultural Meteorology, 26,* 51-65. https://doi.org/10.1016/0002-1571(82)90057-7